Iraqi Journal of Physics, 2023 *Vol. 21, No. 4, PP. 84-91*
https://doi.org/10.30723/ijp.v21i41123. *P-ISSN: 2070-4003*
E-ISSN: 2664-5548

Surface Plasmon Resonance (SPR)-Based Multimode Optical Fiber Sensors for Electrical Transformer Oil Aging Detection

Mariam Jamal Abd Alkareem [1a*] and Soudad S. Ahmed [1b]
[1]*Department of Physics, College of Science, University of Baghdad, Baghdad, Iraq*
[a]E-mail: mariamjamal2411@gmail.com
[a*]Corresponding author: soudadbassam@gmail.com

Abstract

In this study, optical fibers were designed and implemented as a chemical sensor based on surface plasmon resonance (SPR) to estimate the age of the oil used in electrical transformers. The study depends on the refractive indices of the oil. The sensor was created by embedding the center portion of the optical fiber in a resin block, followed by polishing, and tapering to create the optical fiber sensor. The tapering time was 50 min. The multi-mode optical fiber was coated with 60 nm thickness gold metal. The deposition length was 4 cm. The sensor's resonance wavelength was 415 nm. The primary sensor parameters were calculated, including sensitivity (6.25), signal-to-noise ratio (2.38), figure of merit (4.88), and accuracy (3.2). In the current study, the refractive index values of sucrose and water solutions at different concentrations, which were used as a calibration method, were calculated to be (1.346, 1.359, 1.382, and 1.39). It was found that when the refractive index of the sensitive medium increases, the length of the resonant wavelength increases due to the decrease in energy.

Article Info.

Keywords:
Multi-Mode, Optical Fiber, Optical Fiber Sensor, Surface Plasmon Resonance, Electrical Transformer Oil.

Article history:
Received: Apr.15, 2023
Revised: Aug. 08, 2023
Accepted: Oct. 10, 2023
Published: Dec. 01,2023

1. Introduction

Optical fibers are flexible, transparent fibers made by drawing glass (silica) or plastic to a diameter slightly thicker than that of human hair [1-3]. They are used most often as a means to transmit light between the two ends of the fiber and find wide usage in fiber-optic communications, where they permit transmission over longer distances and at higher bandwidths (data transfer rates) than electrical cables [4-7]. Fibers are used instead of metal wires because signals travel along them with less loss; in addition, fibers are immune to electromagnetic interference, a problem from which metal wires suffer [8-11]. They are also used for illuminating and imaging and are often wrapped in bundles, so they may be used to carry light into or images out of confined spaces, as in the case of a fiberscope [12-15]. Specially designed fibers are also used for a variety of applications, such as fiber optic sensors and fiber lasers [16-19].

The essential insulating substance used in electrical power transformers is transformer oil, often known as mineral insulating oil. It is produced via fractional distillation of crude petroleum. In power transformers, this oil performs two key tasks: first, it works as a liquid insulator for electrical purposes, and second, it effectively dissipates heat, serving as a coolant [20].

Transformer oil provides two additional crucial objectives in addition to these primary ones. First of all, because the core and winding are entirely submerged in the oil, it helps to preserve them. Second, it is essential for protecting the cellulose-based paper insulation from the damaging effects of ambient oxygen, which can lead to oxidation.

Water content, kinematic viscosity, flash point, resistivity, and dielectric strength are the material's primary properties. When selecting the proper transformer oil, these

characteristics are carefully taken into account. Higher quality oil is necessary for transformers working under great loads and high voltage. However, utilizing high-quality oil is not strictly necessary for transformers that are lightly loaded and running at low voltages [21].

Updike and Hicks proposed the first biosensor in 1967. There are many different bio-sensing methods accessible today, including optical biosensors [22, 23], electrochemical, thermometric, piezoelectric, and magnetic ones. One of them is optical fiber biosensors based on surface plasmon resonance (SPR), which have been shown to be economically advantageous in the fields of chemistry and the biological sciences [24, 25]. SPR is an effective technique for examining the optical characteristics of nano- and biomaterials [26-28]. To detect the absorption of various compounds on metal films, such as gold (Au) and silver (Ag), SPR sensors employ a variety of devices. Drug discovery, environmental protection, and medical diagnostics are all areas where this technique is useful [29-32]. The investigation of positioner surface plasmon produced by light oscillations of conduction band electrons in metal nanoparticles led to a significant improvement in characteristics. Surface-enhanced chemical-specific sensing resulted from this. Since the discovery of Raman scattering in the 1970s, a novel advance in photochemistry known as surface plasmon-mediated hot carrier generation has also developed [33-35]. SPR based refractive index (RI) sensors are extremely sensitive to even minor changes. They have been thoroughly studied for biochemical sensing applications, such as environmental monitoring, food safety, and disease detection. Due to their accessibility, portability, potential for in-situ and real-time monitoring and cost, optical fiber-based (SPR) sensors have grown in popularity over the years [36-39]. SPR sensor was first introduced by C. Jorgenson et al. in 1993 [40-43], and various investigations have subsequently been conducted on it. Contrary to prism-based on-surface SPR sensors, optical fiber-based on-surface SPR sensors frequently function in the spectrum band modulation mode. Placing the cladding or fiber core up against the quartz prism allows for the coupling of the emitted light to the metal layer. Polarized power is supplied to the metal layer as an evanescent wave to ignite the surface plasmon signal. There are numerous types of fiber-based on SPR sensors that have been created, including hetero-core fiber-based on SPR sensors, SPR sensors with slanted fiber Bragg gratings, fiber-based on SPR sensors with tapering, fiber-based SPR sensors with side polishing [44] fiber-based on SPR sensors with end polishing [45] and long-period fiber-Bragg grating (FBG) based on surface plasmon resonance SPR sensors [46] produce the evanescent wave. These SPR sensors have been built using single-mode fibers, multimode fibers, and microstructure fibers, among other optical fiber types. Due to their small core diameter, single-mode fibers are extremely fragile after tapering or side-polishing. However, due to their larger core diameter and strong mechanical qualities, multimode fibers have improved coupling efficiency with broadband light sources and preserve their mechanical properties even after such procedures. Due to the abundance of guided modes, multimode fibers have a wider SPR bandwidth; however, this bandwidth can be decreased by improving multilayer components or fiber designs [47-50]. In our previous study we used single-mode and multi-mode optical fibers based on surface plasmon resonance to characterize some materials, such as (Candida, hemoglobin, and water pollution). In this work, a multi-mode optical fiber based on surface plasmon resonance was used to detect the age of the oil used in the electrical transformers.

2. Experimental Work

Oil samples of different ages were collected from electrical transformers and generators, and motorcycles before and after combustion.

The experimental set-up is suggested for assessing the bandwidth of the light transmitted by multi-mode fiber (Fig. 1) an optical analyzer (OSA) supplied by Thorlabs Co., and an output unit (PC).

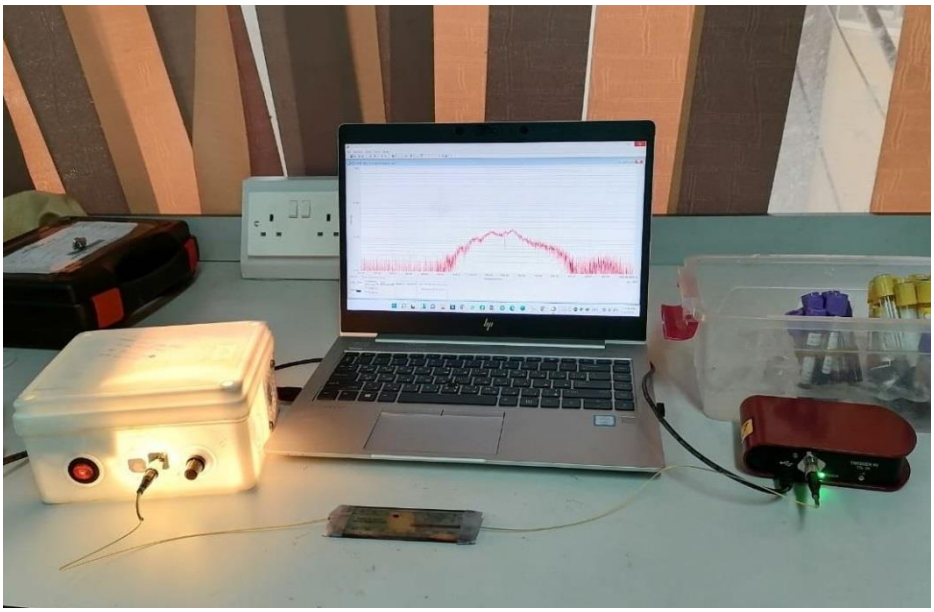

Figure 1: The SPR multi-mode fiber sensor experimental setup.

The sensing region is situated in the middle of the multi-mode optical fiber (Fig. 2). After being cleaned with distilled water, gold is sputtered onto the optical fiber with a thickness of 40 nm.

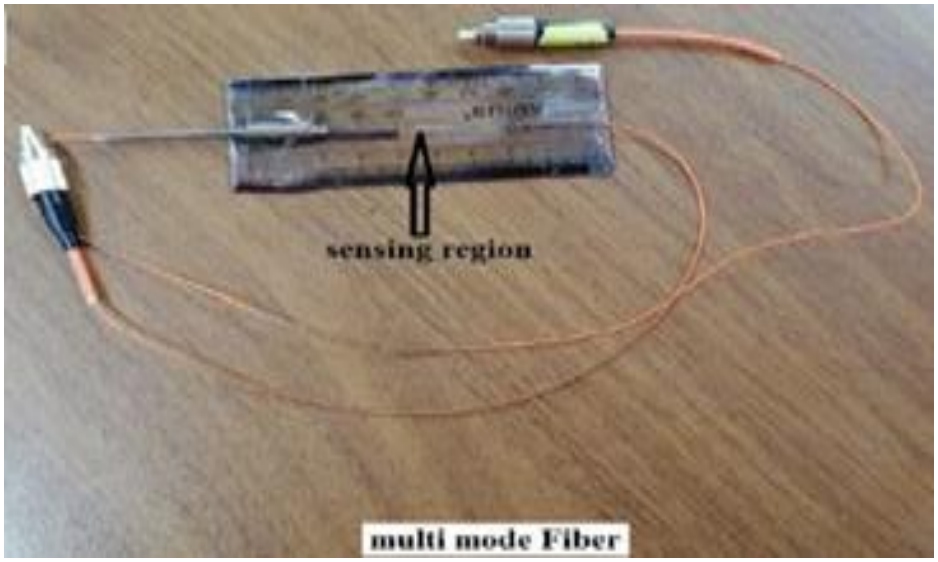

Figure 2: Multi-mode fiber sensor with the coated gold layer.

3. Results and Discussion

3.1. Preparation of Sugar Solutions

To find the SPR calibration curves of the studied sensor, the sensitive zone was immersed in sucrose and water solution at different concentrations (Fig.3), i.e., with different refractive indices. The refractive indices of the solutions were measured using a refractometer (Abbe type).

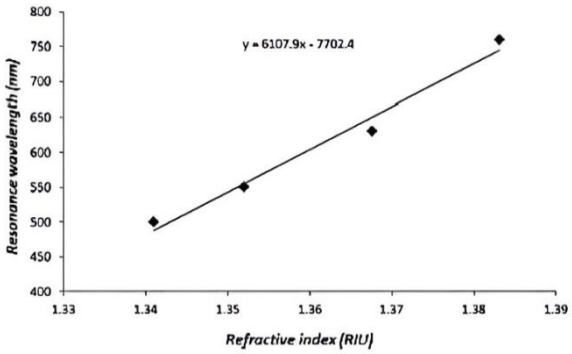

Figure 3: The refractive index as a function of sucrose concentration dissolved in water.

Fig. 4 shows the AFM results of the surface morphology of the Au nanolayer. The result show that there is a significant increase in the surface roughness as the thickness of the Au layer increases. The increase of surface roughness was observed first as the globular structure appeared on the glass. Further increase of the Au thickness led to the increase of the layer's homogeneity and the globular structure being less pronounced as well as the surface roughness.

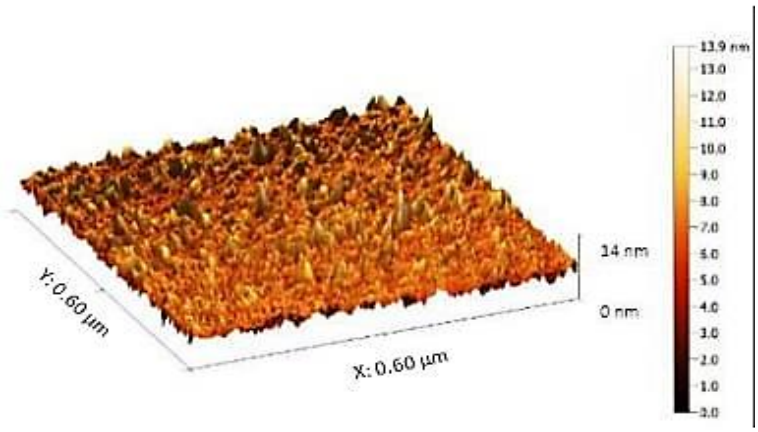

Figure 4: AFM with 60nm Au layer thickness.

Several factors involving multimode fibers with different refractive index values (1.346, 1.359, 1.382, and 1.39) were the optical fiber sensor immersed in sucrose and water solution. Fig. 5: shows that as energy is reduced, the refractive index of the sensor medium rises and the abrupt dip in the resonance wavelength is shifted to the greater wavelength side.

The SPR response curve of the manufactured sensor with a gold layer at different refractive indices for electrical transformer oil (sensitive media) is illustrated in Fig 6a. It's obvious that the resonance wavelength of the multi-mode fiber was shifted from 568 nm to 680 nm as shown in Fig. 6b, and that the refractive index of the transformer oil varied with oil age. The more sediment that forms inside the oil with age increased its refractive index, the higher the refractive index, which causes the redshift (toward higher wavelengths). The result is in agreement with ref. [10].

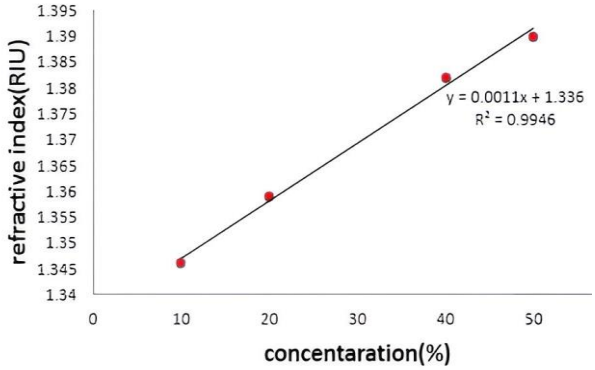

Figure 5: Refractive index against resonance wavelength for the multi-mode fiber sensor with a gold coating.

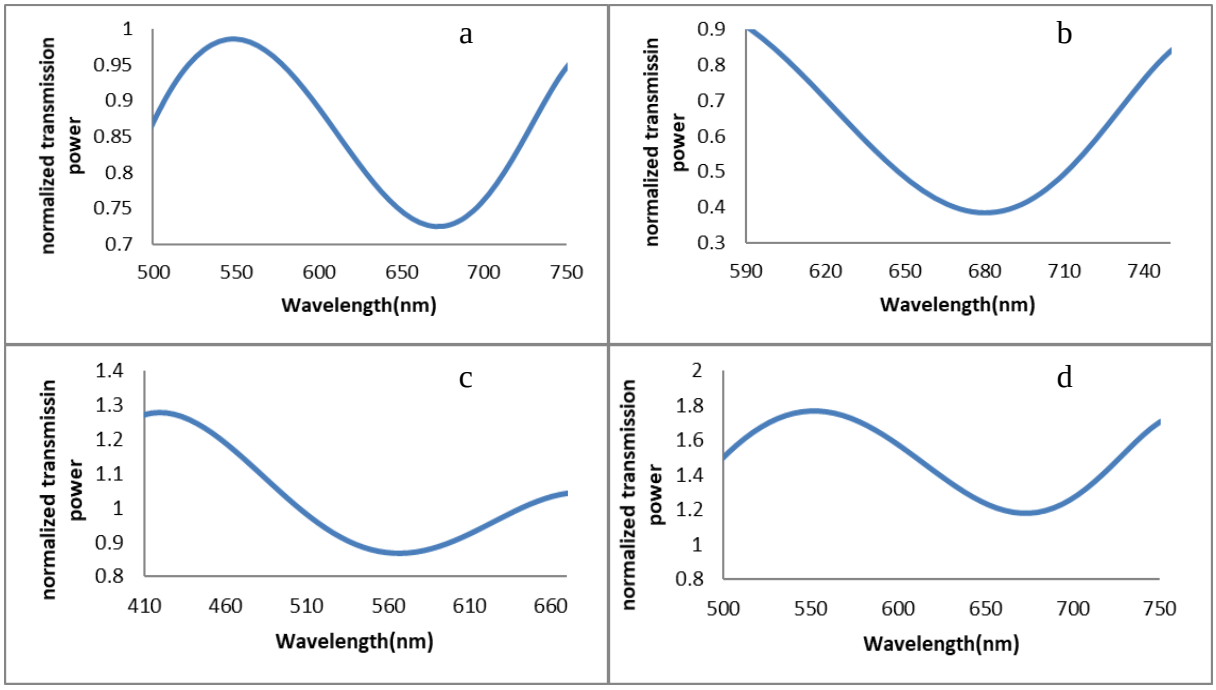

Figure 6: The SPR curves for multi-mode samples before and after the oil combustion.

A good sensor should have a high value of FOM, i.e., a minimum full width at half maximum (FWHM) of the spectrum, whereas the refractive index (RIU) varies with wavelength. Table 1 shows the values and concentrations of the refractive indices at various resonance wavelengths. While Table 2 listed the values of the sensitivity, signal to noise ratio, figure of merit, and resolution.

Table 1: The values and concentrations of the refractive indices at various resonance wavelengths.

Type of fiber	Samples	λ_{res}(nm)	Refractive index (RIU)	Concentration C%
Multi-mode	a	670	1.3707	31.5
	b	680	1.3723	33.0
	c	568	1.3540	16.3
	d	675	1.3715	32.2

Table 2: The sensor with gold's experimental performance metrics.

METAL	Sensitivity (Sn) (μm/ RIU)	Signal to noise ratio (SNR)	Figure of merit (FOM)	Resolution (RIU)
Gold	6.25	2.38	14.88	$3.2x10^{-5}$

The figures show that the λ_{res} was shifted toward the longer wavelength (red shift) after the oil was combusted due to the increase in the refractive index. The sensitivity (nm/RIU) was calculated using the equation ($S= \Delta\lambda_{res} / \Delta n_s$), signal-to-noise ratio (SNR) was calculated using the equation ($SNR= \Delta\lambda_{res} / \Delta\lambda_{0.5}$), the Figure of Merit (FOM) was calculated using the equation ($S/\Delta\lambda_{0.5}$).

4. Conclusions

This study exhibited the application of a multi-mode optical fiber as a chemical sensor based on the SPR technique for estimating the concentration and refractive index of lubrication oil in electrical transformers. The response curve of the sensor for various samples and the resonance position (the dip of the curve) were determined. However, the combustion occurred, the sediment increased and the refractive index. All these factors contributed to the tendency to be closer to higher wavelengths (redshift). The resonance wavelength was changed for each sample of oil, and as a sequence, the refractive index change led to a change in the resonance wavelength value. From the results, the optical fiber-based surface plasmon resonance (SPR) sensor with the 60 nm thick film of gold metal and 4 cm of exposed sensing region was successful in getting performance parameters of the sensitivity approach of 6.25 μm/RIU, signal-to-noise ratio of 2.38, resolution of 10.2×10^{-5} RIU and figure of merit of 14.88.

Acknowledgments

The authors would like to thank the Department of Physics, College of Science, University of Baghdad.

Conflict of Interest

The authors declare that they have no conflict of interest.

References

1. *The fiber optic association, inc. The international professional association of fiber optics*; https://www.thefoa.org/.
2. Y. Zhou, Y.-N. Zhang, B. Han, L. Cheng, D. Li, W. Zheng, and Y. Zhao, Measurement **207**, 112353 (2022).
3. C. Liu, J. Wang, F. Wang, W. Su, L. Yang, J. Lv, G. Fu, X. Li, Q. Liu, and T. Sun, Opt. Communic. **464**, 125496 (2020).
4. S. Lawan, M. Ajiya, and D. Shu'aibu, Signal **10**, 3 (2012).
5. A. H. Malik, M. Azeem, M. Y. Hamza, and S. Tariq, in 2008 Second International Conference on Electrical Engineering (IEEE, 2008). p. 1.
6. M. Hamza and S. Tariq, in 2007 International Conference on Electrical Engineering (Lahore, Pakistan IEEE, 2007). p. 1.
7. A. Razzaq, H. Zainuddin, F. Hanaffi, and R. M. Chyad, IET Sci. Measur. Tech. **13**, 615 (2019).
8. J. M. Senior and M. Y. Jamro, *OPTICAL FIBER COMMUNICATIONS: PRINCIPLES AND PRACTICE* (Harlow, England, Pearson Education, 2009).
9. H. K. Hisham, Am. J. Sens. Tech. **4**, 30 (2017).
10. R. Nasirifar, M. Danaie, and A. Dideban, Optik **250**, 168051 (2022).

11. N. S. Rahim, S. S. Ahmed, and M. F. Sultan, Iraqi J. Sci. **61**, 1650 (2020).
12. M. Azadeh, *FIBER OPTICS ENGINEERING* (Davis, CA, USA, Springer, 2009).
13. N. S. Omar, Y. W. Fen, S. Saleviter, W. M. E. M. M. Daniyal, N. A. Anas, N. S. M. Ramdzan, and M. D. A. Roshidi, Materials **12**, 1928 (2019).
14. V. T. Huong, V. Van Tran, N. Y. Lee, D. Van Hoang, K. T. Loan Trinh, T. B. Phan, and N. H. Thi Tran, Langmuir **36**, 9967 (2020).
15. W. Zheng, B. Han, E. Siyu, Y. Sun, X. Li, Y. Cai, and Y.-N. Zhang, Microchem. J. **157**, 105010 (2020).
16. B. Lee, Optic. Fiber Tech. **9**, 57 (2003).
17. K. Fidanboylu and H. Efendioglu, in 5th International Advanced Technologies Symposium (IATS'09) (Karabuk, Turkey Karabük University, 2009). p. 2.
18. H. K. Hisham, Am. J. Rem. Sens **6**, 1 (2018).
19. R. Nasirifar, M. Danaie, and A. Dideban, Optik **186**, 194 (2019).
20. D. Abeysundara, C. Weerakoon, J. Lucas, K. Gunatunga, and K. Obadage, in ERU Symposium (Bandaranayake Mawatha, Moratuwa University of Moratuwa, 2001). p. 1.
21. F. Sitinjak, I. Suhariadi, and L. Imsak, in Proceedings of the 7th International Conference on Properties and Applications of Dielectric Materials (Cat. No. 03CH37417) (Nagoya, Japan IEEE, 2003). p. 495.
22. E. A. Fadhil, M. M. Abdullah, and F. M. Lafta, Iraqi J. Appl. Phys. **19**, 35 (2023).
23. E. A. Fadhil, M. M. Abdullah, and F. M. Lafta, Int.. J. Nanosci., 2350061 (2023).
24. M. F. Sultan, A. A. Al-Zuky, and S. A. Kadhim, Al-Mustansiriyah J. Sci. **29**, 195 (2018).
25. L. Mescia and F. Prudenzano, Fibers **2**, 1 (2013).
26. E. Kretschmann and H. Raether, Zeitsch. Naturfors. A **23**, 2135 (1968).
27. A. Otto, Zeitsch. Phys. Had. Nuc. **216**, 398 (1968).
28. S. Chakma, M. A. Khalek, B. K. Paul, K. Ahmed, M. R. Hasan, and A. N. Bahar, Sens. Bio-sens. Res. **18**, 7 (2018).
29. V. Yesudasu, H. S. Pradhan, and R. J. Pandya, Heliyon **7**, e06321 (2021).
30. F. F. Abbas and S. S. Ahmed, Iraqi J. Sci. **64**, 658 (2023).
31. D. V. Nesterenko and Z. Sekkat, Plasmonics **8**, 1585 (2013).
32. J. Hottin, E. Wijaya, L. Hay, S. Maricot, M. Bouazaoui, and J.-P. Vilcot, Plasmonics **8**, 619 (2013).
33. B. Foerster, V. A. Spata, E. A. Carter, C. Sönnichsen, and S. Link, Sci. Advan. **5**, eaav0704 (2019).
34. A. I. Mahmood, A. I. Mahmood, and S. S. Ahmed, Iraqi J. Sci. **59**, 1577 (2018).
35. N. Yasser, N. A. Ali, and L. H. Sulaiman, Iraqi J. Sci. **59**, 294 (2018).
36. G. M. Jassam, S. S. Alâ, and M. F. Sultan, Iraqi J. Sci. **61**, 765 (2020).
37. T. Allsop and R. Neal, Sensors **19**, 4874 (2019).
38. A. R. Prado, C. A. Díaz, L. G. Lyra Nunes, J. P. Oliveira, M. C. Guimarães, A. Leal-Junior, M. R. Ribeiro, and M. J. Pontes, Plasmonics **16**, 787 (2021).
39. H. H. Qazi, S. F. Memon, M. M. Ali, M. S. Irshad, S. A. Ehsan, M. R. B. Salim, A. B. B. Mohammad, M. Z. Zulkifli, and M. Idrees, J. Mod. Opt. **66**, 1244 (2019).
40. R. A. Kadhim, A. K. K. Abdul, and L. Yuan, IETE Tech. Rev. **39**, 442 (2022).
41. N. S. Rahim, Iraqi J. Phys. **17**, 41 (2019).
42. G. Soghra, B. Jamal, and M. Bahar, Optik **260**, 169026 (2022).
43. A. Urrutia, J. Goicoechea, and F. J. Arregui, J. Sens. **2015**, 1 (2015).
44. H. Han, D. Hou, N. Luan, Z. Bai, L. Song, J. Liu, and Y. Hu, Sensors **20**, 3911 (2020).
45. Q. Wang, J. Y. Jing, and B. T. Wang, Transac. Instrumen. Measur. **68**, 3350 (2019).

46. A. K. Sharma and C. Marques, IEEE Sens. J. **19**, 7168 (2019).
47. J.-Y. Jing, S.-Y. Li, X.-Z. Wang, Q. Zhu, F.-L. Meng, and Q. Wang, Measurement **140**, 395 (2019).
48. G. M. Jassam, Iraqi J. Phys. **17**, 11 (2019).
49. M. F. Sultan, A. A. Al-Zuky, and S. A. Kadhim, Al-Nahrain J. Sci. **21**, 65 (2018).
50. I. Venditti, Materials **10**, 97 (2017).

متحسس الألياف الضوئية متعدد الأنماط القائم على رنين البلازمون السطحي للكشف عن عمر زيت المحولات الكهربائية

مريم جمال عبد الكريم[1]، سؤدد سلمان احمد[1]
[1]قسم الفيزياء ، كلية العلوم ، جامعة بغداد ، بغداد ، العراق

الخلاصة

في هذا العمل، تم تصميم الألياف الضوئية وتنفيذها كمستشعر كيميائي يعتمد على رنين البلازمون السطحي (SPR) لتقدير مؤشرات الانكسار المختلفة وتركيزات زيت المحولات الكهربائية. يتم إنشاء المتحسس من خلال دمج جزء قصير من الألياف الضوئية في وسط كتلة راتنجية، متبوعًا بالتلميع والألياف الضوئية متعددة الأوضاع مدببة لإنشاء متحسس الألياف الضوئية.، وقت المتحسس المدبب هو 50 دقيقة. باستخدام الألياف الضوئية متعددة الأوضاع المودعة بواسطة ترسيب معدن ذهبي بسمك 60 نانومتر لمنطقة المتحسس لحساس 4 سم وطول موجة الرنين 415 نانومتر للمتحسس. بينما يتم حساب معلمات المتحسس الأساسي، بما في ذلك الحساسية، ونسبة الإشارة إلى الضوضاء، ورقم الكفاءة، والدقة، والقيم رقم الكفاءة هي 14.88، ونسبة الإشارة إلى الضوضاء هي 2.38، والحساسية 6.25، والدقة هي 3.2 في العمل الحالي، تم اكتشاف عدد من المتغيرات التي تتضمن الألياف متعددة الأنماط وأرقام معامل الانكسار المتغيرة (1.346، 1.359، 1.382، و1.39) في سائل السكروز والماء. وجد أنه عندما يزداد معامل الانكسار للوسط الحساس يزداد طول الموجة الرنينية بسبب نقص الطاقة.

الكلمات المفتاحية: متعدد الانماط، ليف بصري، متحسس الليف البصري، رنين البلازمون السطحي، زيت المحولات الكهربائية.